Journal of Hydrology 564 (2018) 1153–1164

Contents lists available at ScienceDirect

Journal of Hydrology

journal homepage: www.elsevier.com/locate/jhydrol

Research papers

Frozen ground degradation may reduce future runoff in the headwaters of an inland river on the northeastern Tibetan Plateau

Yuhan Wang[a], Hanbo Yang[a], Bing Gao[b], Taihua Wang[a], Yue Qin[a], Dawen Yang[a,*]

[a] State Key Laboratory of Hydroscience and Engineering, Department of Hydraulic Engineering, Tsinghua University, Beijing 100084, China
[b] School of Water Resources and Environment, China University of Geosciences, Beijing 100083, China

ARTICLE INFO

This manuscript was handled by Marco Borga, Editor-in-Chief, with the assistance of Kelly Kibler, Associate Editor

Keywords:
Increasing air temperature
Frozen ground
Runoff change
Distributed ecohydrological model
Heihe River Basin

ABSTRACT

On the Tibetan Plateau, climate change, particularly increases in air temperature, significantly affects cryospheric and hydrological processes. Based on 5 typical future climate scenarios from the Coupled Model Intercomparison Project (CMIP5) under emission scenario RCP4.5 and a distributed ecohydrological model (GBEHM), this study analyzes the potential characteristics of future climate change (from 2011 to 2060) and the associated effects on the cryospheric and hydrological processes in the upper Heihe River Basin, a typical cold mountain region located on the northeastern Tibetan Plateau. The precipitation, air temperature, and frozen ground elasticities of runoff/evapotranspiration are then estimated based on the simulation results. The typical future climate scenarios suggest that air temperature will increase at an average rate of 0.34 °C/10a in the future and that precipitation will increase slightly by 6 mm/10a under the RCP 4.5 emission scenario. Based on the GBEHM-simulated results, due to the increase in air temperature, glaciers would be reduced to less than 100 million m^3 by 2060, the permafrost area would shrink by 23%, the maximum frozen depth of seasonally frozen ground would decrease by 5.4 cm/10a and the active layer depth of the frozen ground would increase by 6.1 cm/10a. Additionally, runoff would decrease by approximately 5 mm/10a, and evapotranspiration would increase by approximately 9 mm/10a. The estimated elasticities indicate that annual runoff would decrease at an average rate of 24 mm/°C and evapotranspiration would increase at an average rate of 21 mm/°C with rising air temperature in the future. The impacts of increased air temperature on hydrological processes are mainly due to changes in frozen ground. The thickening of the active layer of the frozen ground increases the soil storage capacity, leading to decreased runoff and increased evapotranspiration. When the active layer depth increases by 1 cm, annual runoff decreases by approximately 1.3 mm, and annual evapotranspiration increases by approximately 0.9 mm. In addition, the shift from permafrost to seasonal frozen ground increases groundwater infiltration, which decreases surface runoff. Compared to that over the past 50 years, the effect of increased air temperature on the frozen ground in the upper Heihe River Basin will be greater in the future, which would result in a faster reduction in runoff in the future considering the effects of global warming.

1. Introduction

The Tibetan Plateau, as the source area of many major Asian rivers, provides valuable freshwater resources for hundreds of millions of people in China and Southeast Asian countries (Immerzeel et al., 2010). Due to its unique geography, the Tibetan Plateau is more sensitive to global climate change than other areas (Bales et al., 2006; Cheng and Wu, 2007). In recent decades, rivers on the Tibetan Plateau have experienced significant but different runoff changes due to climate change (Cuo et al., 2014). On the eastern Tibetan Plateau, which is controlled by the East Asian Monsoon, runoff has decreased (Yang et al., 2011), and in the region mainly controlled by the westerly belt, runoff has increased (Cheng and Jin, 2013). Will these trends continue or change in the future? To develop reasonable water resource management strategies, it is important to reasonably estimate the trends of river runoff.

Unlike other regions, the Tibetan Plateau is widely covered by permafrost and glaciers. Previous studies have shown that in addition to the changes in temperature and precipitation, cryospheric changes, such as variations in glacier coverage and the area of frozen ground, have had important and far-reaching effects on the ecological and hydrological processes in the basin (Barry and Gan, 2011; Immerzeel et al., 2012; Cuo et al., 2014). Accelerated glacial ablation can increase surface runoff, reduce water reserves and change the surface albedo,

* Corresponding author.
E-mail address: yangdw@tsinghua.edu.cn (D. Yang).

https://doi.org/10.1016/j.jhydrol.2018.07.078
Received 16 January 2018; Received in revised form 29 May 2018; Accepted 27 July 2018
Available online 31 July 2018
0022-1694/ © 2018 Elsevier B.V. All rights reserved.

and permafrost degradation can alter the soil moisture content, soil water storage capacity and other hydrological elements (Cuo et al., 2015). In recent decades, global warming has led to the substantial retreat of frozen ground and glaciers on the Tibetan Plateau (Yao et al., 2007; Kang et al., 2010; Cheng and Jin, 2013). In the past 30 years, the permafrost area of the Tibetan Plateau has been reduced from 1.50×10^6 km^2 to 1.05×10^6 km^2, and the permafrost degradation trend may continue or even accelerate in the future (Cheng and Jin, 2013). According to the First and Second Glacier Inventory Datasets of China (Guo et al., 2014), the glacier area on the Tibetan Plateau retreated by 23% over the past 50 years. These changes will further affect the hydrological cycle. Therefore, to reliably predict future runoff trends, it is important to answer the following 3 questions.

(1) How will the cryospheric response vary for typical future climate change scenarios?
(2) How will climate change effect hydrological processes, and what factors cause changes to glacier and frozen soil regimes?
(3) Can these influences be quantified?

Previous studies have lacked the ability to estimate cryospheric changes in the context of future climate change, and analyses of the impacts of cryospheric changes on hydrological processes have not been conducted.

Distributed hydrological models that consider cryospheric processes are the major tools used to estimate the spatial distribution and dynamic variations of cryospheric and hydrological processes. In previous studies, models such as MIKE-SHE (Bosson et al., 2012), CLM (Lawrence et al., 2015), WEB-DHM (Wang et al., 2010), and VIC (Cuo et al., 2015) considered the effects of cryospheric processes. However, in most of these studies, frozen ground was considered a static layer. The dynamic changes in frozen ground and the interactions between frozen ground and hydrological processes were not effectively considered (Qin et al., 2016). Yang et al. (2015) developed a distributed ecohydrological model (GBEHM) that fully couples cryospheric processes. With this model, the spatial distribution and dynamic variations of glaciers and frozen soils can be simulated (Gao et al., 2016). GBEHM has been applied in certain river basins on the Tibetan Plateau, such as the Heihe River Basin (HRB) and upper Yellow River Basin, and the cryospheric and hydrological processes in recent decades were successfully simulated (Yang et al., 2015; Qin et al., 2016). Based on the model, the responses of cryospheric and hydrological processes to climate change in the future can be analyzed.

Future climate scenarios are mainly derived from the simulation results of general circulation models (GCMs; Fowler et al., 2007). In general, GCM simulations often have bias compared to measured values; therefore, bias correction is needed. Due to the lack of gauge observations, future simulation results must be corrected based on the relationship between historical data and historical model simulation results (Wood et al., 2004). Three bias correction methods have mainly been used in previous studies, including the delta method, the unbiasing method and the quantile-quantile mapping method (Gao, 2012). The quantile-quantile mapping method has been widely adopted (Boé et al., 2007). In addition to bias, another problem associated with GCM simulations is their low spatial resolution. The original GCM outputs cannot meet the requirements of high spatial resolution hydrological simulations (Wood, 2002, 2004), and a spatial downscaling process is necessary. Among statistical downscaling and dynamic downscaling methods, statistical downscaling methods are simple and more applicable when historical observations are abundant (Gao, 2012).

The HRB, which is located on the northeastern Tibetan Plateau, is the second largest inland river basin in China. It flows through the Hexi Corridor, which is the most important route from northern China to central Asia for traders and the military and an essential grain-producing region in northwestern China (Zhang et al., 2016a). The water resources required for socioeconomic development and the sustainment of ecosystems in the middle and lower reaches of the basin are heavily dependent on the water from the headwater region. The headwater region of the Heihe River is covered by frozen ground. Specifically, this area is the junction area of permafrost and seasonal frozen soil (Wang et al., 2013), which is sensitive to climate change (Cuo et al., 2015). The HRB has been considered a typical region for scientists to study the hydrology and water resources of cold and arid regions in China (Ning et al., 2008).

This study assesses the potential climate changes based on the outputs of GCMs and the associated influences on the cryospheric and hydrological processes in the HRB from 2011 to 2060 using a distributed hydrological model. The objectives of this study are as follows: (i) to estimate the possible climate changes in the HRB over the next 50 years; (ii) to estimate the responses of cryospheric and hydrologic processes (especially runoff) to future climate change; and (iii) to quantitatively analyze the effects of precipitation, air temperature and frozen ground changes on runoff.

2. Study area and data

2.1. Study area

The HRB originates on the north slope of the Qilian Mountains located on the northeastern Tibetan Plateau, flows through the Hexi Corridor and ends in Juyanhai Lake (Fig. 1). The upper reach of the Heihe River is located at an elevation of 1800–5000 m and gauged at Yingluoxia hydrological station. The river has a drainage area of 10,009 km^2 and generates nearly 70% of the total runoff in the basin (Yang et al., 2015). In the 2000s, the mean annual runoff observed at Yingluoxia station was approximately 1.8 billion m^3.

The annual precipitation in the upper HRB ranges from 200 to 700 mm, and the annual mean air temperature ranges from −9 to 5 °C. Precipitation and temperature are significantly affected by the elevation of the upper HRB (precipitation increases with elevation, and temperature decreases with elevation; Wang et al., 2017), which also leads to the significant spatial variability in land use/cover (Gao et al., 2016). Low-elevation areas are relatively arid and mainly distributed with seasonal frozen soils. As elevation and precipitation increase, water becomes more abundant, and vegetation types and cover increase. The elevation zone of 2800 m–3600 m is the most vegetated area in the basin (Gao et al., 2016). As the elevation continues to increase, the temperature drop leads to sparse vegetation. The 3600–3900 m elevation range is mainly the transition zone from

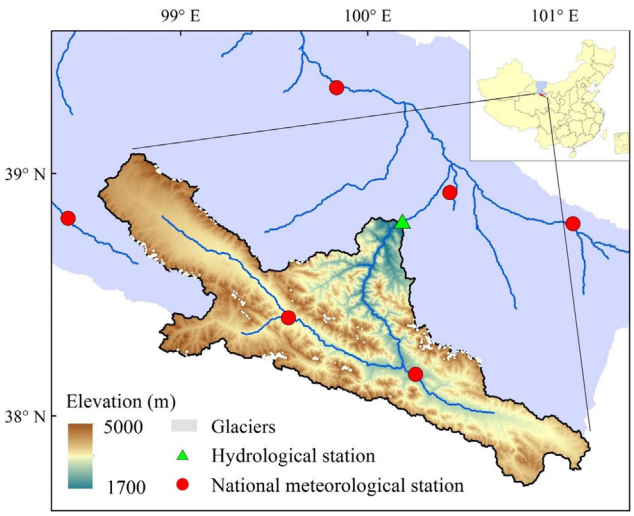

Fig. 1. Study area and the spatial distribution of the long-term mean annual precipitation and annual mean air temperature.

Table 1
Description of the applied GCMs and the trends of the simulated precipitation and air temperature in the future 5 decades (2011–2060) under the RCP4.5 scenario.

GCM	Institution	Spatial resolution	Precipitation trend (mm/10a)	Air temperature trend (°C/10a)
BCC-CSM1.1 (m)	Beijing Climate Center, China	320*160	−1.1	0.28*
CSIRO-Mk3.6.0	CSIRO in collaboration with Queensland Climate Change Centre of Excellence, Australia	192*96	7.4*	0.42*
IPSL-CM5A-MR	L'Institut Pierre-Simon Laplace, France	144*143	15.0*	0.34*
CNRM-CM5	Centre National de Recherches Météorologiques/Centre Européen de Recherche et de Formation Avancée en Calcul Scientifique, France	256*128	12.3*	0.27*
MPI-ESM-LR	Max Planck Institute (MPI) for Meteorology, Germany	192*96	−5.9	0.40*

Note: "*" in precipitation trend and air temperature trend means significant trends ($\alpha = 0.1$).

permafrost to seasonal frozen soil (Gao et al., 2018). In addition, the area above 4000 m is mainly the permafrost area and includes a few glaciers. As the temperature has increased in recent decades, the glaciers and frozen grounds in the upper HRB have become significantly degraded (Gao et al., 2018). Until 2010, the total glacier area was approximately 80 km^2, and the total associated water reserve was approximately 0.5 billion m^3 (according to the Second Glacier Inventory Dataset of China, Guo et al., 2014).

2.2. Data used in the study

(1) GCM data

The GCMs used in the study were selected from 47 GCMs in the Coupled Model Intercomparison Project (CMIP5, http://cmip-pcmdi.llnl.gov/cmip5/). Hu et al. (2014) evaluated the precipitation and temperature of 44 GCMs from CMIP5 on the Tibetan Plateau and recommended 19 of them. Zhang et al. (2016a) adopted a method proposed by Fu et al. (2013) to evaluate the outputs of the 47 GCMs in the HRB. Based on these evaluations, we selected 5 GCMs with relative high spatial accuracy (see Table 1) from the recommended GCMs. Fig. 2 compares the simulated historical annual precipitation and air temperature of the GCMs with observations. The data show that the simulated precipitation estimates are similar to the observations (relative error of less than 20%). However, the 5 GCMs overestimate the air temperature in the upper HRB. This system bias is corrected based on the quantile-quantile mapping method (introduced in Section 3.1). Fig. 2 also shows that the historical air temperature trends simulated by the GCMs are close to the observed values, as shown in Table 1. The GCM-simulated values of daily precipitation, mean/maximum/minimum air temperature, wind speed and relative humidity under emission scenarios RCP2.6, RCP4.5 and RCP8.5 were adopted in this study.

(2) Historical precipitation, air temperature and runoff

Historical 1-km gridded precipitation and air temperature data (from 1981 to 2010) were used as references to correct the future climate data. The historical precipitation data were derived from a 3-km resolution gridded daily precipitation dataset and resampled to 1-km grids (the spatial resolution required by the ecohydrological model) (Wang et al., 2017). The historical air temperature data were interpolated by observations from meteorological stations using an angular distance weighting (ADW) interpolation method (Willmott et al., 1985; New et al., 2000; Yang et al., 2004), and the interpolation considered the temperature gradient with elevation. Additionally, the historical runoff data observed at the Yingluoxia station were used for comparison with the simulated future runoff.

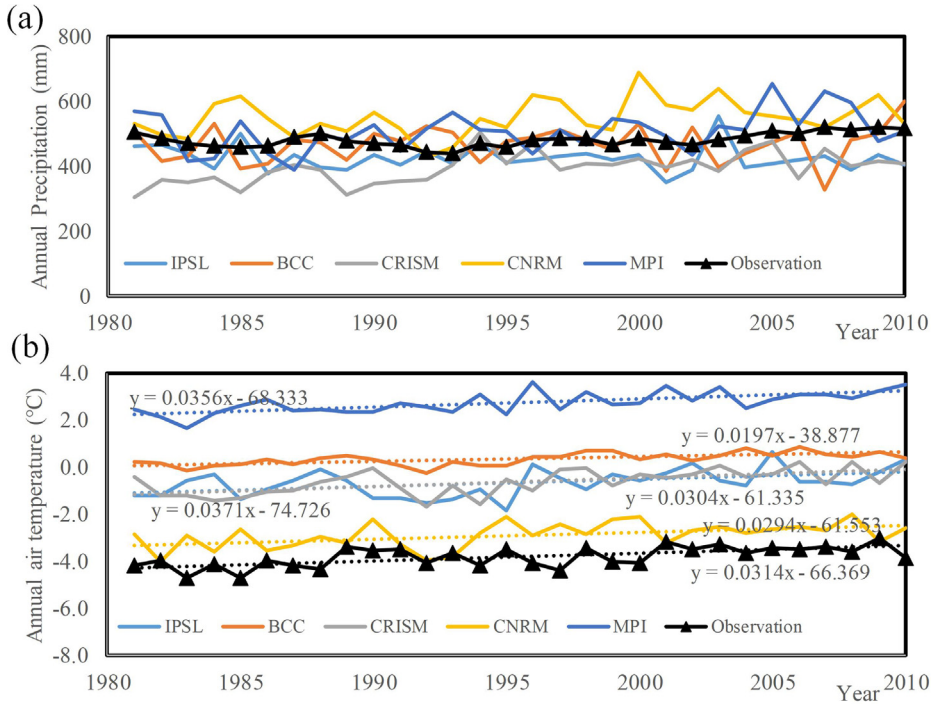

Fig. 2. Simulated historical (1981–2010) (a) annual precipitation and (b) annual mean air temperature based on different GCMs in comparison to observed values.

(3) Other geographical data

Topography, land use, soil parameters and leaf area index (LAI) data are required to build a distributed ecohydrological model. The topography data were obtained from the SRTM dataset (Jarvis et al., 2008). The land use data were provided by the Institute of Botany, Chinese Academy of Sciences (Zhou and Zheng, 2014). The soil parameters, including the hydraulic conductivity, residual soil moisture content and saturated soil moisture content, were derived from a 1-km dataset developed by Song et al. (2016). The historical LAI data were derived from an LAI dataset produced by Fan (2014), and in this study, we assumed that the future LAI equals the average of the corresponding values from 2001 to 2010.

3. Methods

3.1. Statistical downscaling of GCM outputs

We adopted a bias correction and spatial downscaling (BCSD) method for statistically downscaling the GCM-simulated precipitation and air temperature (Wood, 2002, 2004). This method includes two major steps: bias correction and spatial downscaling. Bias correction is implemented based on the quantile-quantile mapping method. For a given variable (such as the precipitation or air temperature), the cumulative density function (CDF) of the control simulation (i.e., historical simulation) is first matched with the CDF of the observation, and a correction function is generated depending on the quantile. Then, this correction function is used to correct the variable (historical and future simulations) in a quantile-by-quantile process (Boé et al., 2007). We assume that the CDFs of the observations and historical GCM simulations are $F_1(X)$ and $F_2(X)$, respectively. Then, we correct the GCM simulation $Xsim$ to $Xcor = F_1^{-1}(F_2(Xsim))$. Bias correction is applied at the spatial scale of the GCM output (for convenience, we define the grid scale of GCM output as a "large scale"). Then, the corrected values are spatially downscaled to a "small scale", which is required by the hydrological model (1 km in this study). We first define the adjustment coefficient of the large-scale grid (m, n) as $f_{T(m,n)} = Xcor_{m,n} - \overline{Xobs_{m,n}}$ (for air temperature) and $f_{P(m,n)} = Xcor_{m,n}/\overline{Xobs_{m,n}}$ (for precipitation), where $\overline{Xobs_{m,n}}$ denotes the long-term mean observed value. Then, we spatially interpolate (resample) the adjustment coefficients (f_T and f_P) to the small scale using the ADW interpolation method (Willmott et al., 1985; New et al., 2000; Yang et al., 2004). Finally, the corrected simulation results for the small-scale grid (u, v) are calculated as $Xcor_{u,v} = \overline{Xobs_{u,v}} + f_{T(u,v)}$ (for temperature) and $Xcor_{u,v} = \overline{Xobs_{u,v}} \cdot f_{P(u,v)}$ (for precipitation).

3.2. Geomorphology-based ecohydrological model (GBEHM)

GBEHM was developed to simulate hydrological processes by considering the cryospheric processes in cold regions (Gao et al., 2016). In the model, glacier melting is calculated based on an energy balance equation (Gao et al., 2018):

$$Q_M = SW(1-\alpha) + LW_{in} - LW_{out} - Q_H - Q_L - Q_G + Q_R, \quad (1)$$

where Q_M is the net energy absorbed by the surface of the glacier (W/m^2); SW is the incoming shortwave radiation (W/m^2); α is the surface albedo; LW_{in} is the incoming longwave radiation (W/m^2); LW_{out} is the outgoing longwave radiation (W/m^2); Q_H is the sensible heat flux (W/m^2); Q_L is the latent heat flux (W/m^2); Q_G is the penetrating shortwave radiation (W/m^2); and Q_R is the energy from rainfall (W/m^2). Soil freezing and thawing processes are simulated based on the calculation of the energy balance in the soil layer (Gao et al., 2018):

$$C_s\frac{\partial T}{\partial t} - \rho_i L_f \frac{\partial \theta_i}{\partial t} - \frac{\partial}{\partial z}\left(\lambda_s \frac{\partial T}{\partial z}\right) + \rho_l c_l \frac{\partial q_l T}{\partial z} = 0, \quad (2)$$

where C_s is the volumetric soil heat capacity (J·m^{-3}·K^{-1}); T is the temperature (K) of the soil layers; t is time (s); z is the vertical depth of the soil (m); ρ_i is the density of ice (kg/m^3); L_f is the latent heat of fusion (J/kg); θ_i is the volumetric ice content; λ_s is the thermal conductivity (W·m^{-1}·K^{-1}); ρ_l is the density of liquid water (kg/m^3); c_l is the specific heat of liquid water (J·kg^{-1}·K^{-1}); and q_l is the water flux between different soil layers (m/s). The model fully couples the soil freeze-thaw process and hydrological processes. The freeze-thaw process affects soil infiltration, which further effects additional hydrological processes.

In terms of the runoff production mechanism, the model distinguishes between saturation-excess runoff and infiltration-excess runoff. Surface runoff is calculated based on excess infiltration or the exceedance of soil saturation (Yang et al., 2015). The calculation of subsurface flow considers the difference between the saturated zone and unsaturated zone. Flow in the saturated zone is calculated based on a mass balance equation and Darcy's law, and flow in the unsaturated zone is described using the one-dimensional Richards' equation (Yang et al., 2002). The details of GBEHM can be found in recent studies by Yang et al. (2015), Gao et al. (2016), Qin et al. (2017), and Gao et al. (2018).

Yang et al. (2015) and Gao et al. (2016) applied GBEHM in the upper HRB with the support of an integrated research project under the major research plan of "the Integrated Research on the Ecohydrological Processes of the Heihe River Basin," which has been funded by the National Natural Science Foundation of China since 2010. Based on the model, hydrological processes and cryospheric processes in the upper HRB over the past 50 years (1961–2010) were successfully simulated and validated (Yang et al., 2015; Gao et al., 2018). Moreover, the ecohydrological processes, spatial patterns of water balance components, the effects of frozen soil degradation on the hydrological processes were analyzed in detail, as were other relevant issues (Gao et al., 2016, 2018). In the present study, the cryospheric and hydrological responses to future climate change from 2011 to 2060 are simulated based on GBEHM. The model parameters are consistent with those used in the historical simulation calibrated by Gao et al., (2016, 2018), and the initial conditions of the simulation in this study are adopted as the historical simulation results for 2010.

3.3. Attribution analysis of the hydrological changes

In this study, we mainly focus on the impacts of future precipitation and air temperature changes and ignored the changes in other climate factors, such as solar radiation. We also neglect changes in land use/cover (e.g., vegetation) in the study area. The effects of precipitation and air temperature changes on runoff and evapotranspiration are quantified using a climate elasticity model (Fu, 1981; Schaake, 1990; Sankarasubramanian et al., 2001; Chiew et al., 2006; Yang and Yang, 2011; Konapala and Mishra, 2016). The impacts of precipitation and air temperature changes on runoff and evapotranspiration can be calculated as follows:

$$\frac{\Delta R_i}{\overline{R}} = \varepsilon_{P,R}\frac{\Delta P_i}{\overline{P}} + \varepsilon_{T,R}\frac{\Delta T_i}{|\overline{T}|} \quad (3)$$

$$\frac{\Delta ET_i}{\overline{ET}} = \varepsilon_{P,ET}\frac{\Delta P_i}{\overline{P}} + \varepsilon_{T,ET}\frac{\Delta T_i}{|\overline{T}|} \quad (4)$$

where i is the year number; ΔR_i, ΔP_i, ΔT_i, and ΔET_i are the changes in annual mean runoff R_i, precipitation P_i, air temperature T_i and evapotranspiration ET_i compared to the long-term mean values of $\overline{R}$, $\overline{P}$, $\overline{T}$ and $\overline{ET}$, respectively; and $\Delta R_i/\overline{R}$, $\Delta P_i/\overline{P}$, $\Delta T/|\overline{T}|$ and $\Delta ET/\overline{ET}$ are the normalized values of the differences. Because the long-term mean air temperature in the upper HRB is approximately -2 °C, the normalization of ΔT_i is $\Delta T/|\overline{T}|$. $\varepsilon_{P,R}$ and $\varepsilon_{T,R}$ are the precipitation and air temperature elasticities of runoff, and $\varepsilon_{P,ET}$ and $\varepsilon_{T,ET}$ are the precipitation and air temperature elasticities of evapotranspiration, respectively (Ma et al., 2010).

To clearly express the contributions of precipitation and air temperature changes to runoff and evapotranspiration changes, Eqs. (3) and (4) can be rewritten in the following forms:

$$\Delta R_i = \Delta R_{i,P} + \Delta R_{i,T} = \varepsilon'_{P,R}\cdot\Delta P_i + \varepsilon'_{T,R}\cdot\Delta T_i \quad (5)$$

$$\Delta ET_i = \Delta ET_{i,P} + \Delta ET_{i,T} = \varepsilon'_{P,ET}\cdot\Delta P_i + \varepsilon'_{T,ET}\cdot\Delta T_i \quad (6)$$

where $\Delta R_{i,P}$, $\Delta R_{i,T}$, $\Delta ET_{i,P}$ and $\Delta ET_{i,T}$ are the runoff change caused by a precipitation change, runoff change caused by an air temperature change, evapotranspiration change caused by a precipitation change and evapotranspiration change caused by an air temperature change, respectively. Additionally, $\varepsilon'_{P,R} = \varepsilon_{P,R}\cdot\frac{\overline{R}}{\overline{P}}$, $\varepsilon'_{T,R} = \varepsilon_{T,R}\cdot\frac{\overline{R}}{|\overline{T}|}$, $\varepsilon'_{P,ET} = \varepsilon_{P,ET}\cdot\frac{\overline{ET}}{\overline{P}}$ and $\varepsilon'_{T,ET} = \varepsilon_{T,ET}\cdot\frac{\overline{ET}}{|\overline{T}|}$ are the new forms of the elasticities, which reflect the changes in runoff or evapotranspiration when precipitation or the air temperature changes by one unit (1 mm for precipitation and 1 °C for air temperature). In this study, the future elasticities are compared with the historical values to assess whether the elasticities change in the future.

The effects of air temperature changes on runoff and evapotranspiration can be divided into two major categories: potential evaporation changes and cryospheric changes (we assume potential evaporation changes are mainly caused by temperature changes because variations in solar radiation are ignored). Due to the scarcity of glaciers in the upper HRB, the cryospheric changes are mainly reflected by the changes in frozen soil (Wang et al., 2015). Moreover, one possible mechanism that influences changes in frozen ground and the related hydrological processes is the thickening of the active layer, which increases the soil moisture capacity (Wang et al., 2015). Therefore, in Eqs. (5) and (6), the effects of air temperature changes on runoff ($\Delta R_{i,T}$) and evapotranspiration ($\Delta ET_{i,T}$) are divided into $\Delta R_{i,T} = \Delta R_{i,PET} + \Delta R_{i,D}$ and $\Delta ET_{i,T} = \Delta ET_{i,PET} + \Delta ET_{i,D}$, respectively, where subscript *PET* represents the impact of a potential evaporation change and subscript *D* represents the impact of a change in the depth of the active layer. Consequently, Eqs. (5) and (6) can be revised as follows:

$$\Delta R_i = \Delta R_{i,P} + \Delta R_{i,PET} + \Delta R_{i,D} = \varepsilon'_{P,R}\cdot\Delta P + \varepsilon'_{PET,R}\cdot\Delta PET_i + \varepsilon'_{D,R}\cdot\Delta D_i \quad (7)$$

$$\Delta ET_i = \Delta ET_{i,P} + \Delta ET_{i,PET} + \Delta ET_{i,D} = \varepsilon'_{P,ET}\cdot\Delta P + \varepsilon'_{PET,ET}\cdot\Delta PET_i + \varepsilon'_{D,ET}\cdot\Delta D_i \quad (8)$$

where ΔPET and ΔD_i are the differences in annual mean potential evaporation PET_i and the active layer depth D_i compared to the long-term mean values $\overline{PET}$ and $\overline{D}$, respectively. Additionally, $\varepsilon'_{PET,R}$, $\varepsilon'_{D,R}$, $\varepsilon'_{PET,ET}$ and $\varepsilon'_{D,ET}$ are elasticities that represent the changes in runoff or evapotranspiration when potential evaporation or the active layer depth changes by one unit (1 mm for potential evaporation and 1 cm for the active layer depth).

4. Results

4.1. The future climate in the upper HRB

Table 1 provides the precipitation and air temperature trends (after bias correction and downscaling) over 50 years (2011–2060) based on the 5 GCM outputs, which represent 5 future climate scenarios. The future climate scenarios given by CSIRO-Mk3.6.0 and MPI-ESM-LR yield rates of temperature increase higher than the historical trend, and the future precipitation trends are different. Notably, CSIRO-Mk3.6.0 produces a significant increasing trend, and MPI-ESM-LR obtains a decreasing trend. BCC-CSM1.1(m), IPSL-CM5A-MR, and CNRM-CM5 yield rates of increases in the air temperature that are lower than (or similar with) the historical trend. IPSL-CM5A-MR and CNRM-CM5 simulate significant increasing trends for future precipitation, and BCC-CSM1.1(m) displays a slight decreasing trend.

Fig. 3 presents the annual sequences of future precipitation and air temperature. Generally, the upstream portion of the HRB is expected to warm at an average rate of 0.34 °C/10a, and precipitation is expected to experience a slight increasing trend of 5.9 mm/10a. The average rate of air temperature increase of 0.34 °C/10a is close to the estimation of the average warming rate in the HRB (or northeastern Tibetan Plateau) under the RCP4.5 emission scenario in previous studies (Su et al., 2016; Zhang et al., 2016a).

4.2. Changes in glaciers and the frozen soils under future climate scenarios

Table 2 shows the changes in glaciers and frozen soils from 2011 to 2060 based on GBEHM outputs. The results show that for rising temperatures, glaciers will largely disappear by 2060 (to less than 100 million m^3). In this study, permafrost and seasonal frozen ground are distinguished according to the soil temperature. A grid cell was characterized as permafrost when the simulated soil temperature was at or below 0 °C for at least two consecutive years (Woo, 2012; Gao et al., 2018). In 2010, the simulated permafrost area was approximately 5800 km^2 (Gao et al., 2018). In the future 50 years, the permafrost area is projected to shrink by approximately 25% (17%–34% based on different climate scenarios). Fig. 4 shows the spatially averaged monthly ground temperature from 2011 to 2060 in the elevation range between 3600 and 3900 m, which is the transition zone from permafrost to seasonal frozen ground. The results were calculated as the mean value of simulations based on the 5 GCMs. The result indicate that the simulated ground temperature displays a significant increasing trend, and the transition from permafrost to seasonally frozen ground is obvious. In the 2010s, permafrost and the active layer depth were relatively stable. Beginning in the 2020s, permafrost starts to degrade to seasonal frozen ground. In addition to decreases in the permafrost area, the future degradation of frozen soil is also observed based on the decrease in the maximum thickness of seasonally frozen ground (MTSFG) and the thickening of the active layer of the permafrost. The maximum frozen depth of seasonally frozen ground displays a significant decreasing trend of approximately 5.4 cm/10a (3.0–6.7 cm/10a for different climate scenarios), and the active layer depth will significantly increase by approximately 6.1 cm/10a (3.4–8.5 cm/10a for different climate scenarios). Fig. 5 presents the changes in the MTSFG and active layer depth of the permafrost from 2011 to 2060 (mean value of the simulation results of 5 GCMs).

4.3. Changes in the annual water balance under future climate scenarios

Fig. 6 shows the changes in simulated runoff and evapotranspiration in the future 50 years based on different GCMs. Because of the uncertainty in the future climate, the results are not directly expressed by annual runoff and evapotranspiration but by 5-year moving average values. Based on the results, annual runoff exhibits a decreasing trend, and annual evapotranspiration displays a significant increasing trend. On average, annual runoff is expected to be reduced by approximately 5 mm/10a, and the decreases mainly occur in the 2010s and around approximately 2050. By the end of the 2050s, the runoff is expected to be only approximately 1.4 billion m^3, or approximately 80% of the runoff in the 2000s. Evapotranspiration is expected to increase by approximately 9 mm/10a, mainly in the 2010s, 2030s and 2050s. This finding is consistent with the changes in the MTSFG and active layer depth of the permafrost, indicating that the thinning of the frozen layer and thickening of the active layer may have important effects on evapotranspiration. In addition, annual fluctuations in simulated runoff and evapotranspiration based on different GCMs are different, although the long-term trends are similar.

Table 3 shows the average water balance components over the next 50 years based on different GCMs in comparison to the values over the past 30 years (1981–2010, simulated by Gao et al., 2016). Precipitation is clearly more abundant in the next 50 years (486–518 mm based on different GCMs, 498 mm on average) than in the past 30 years

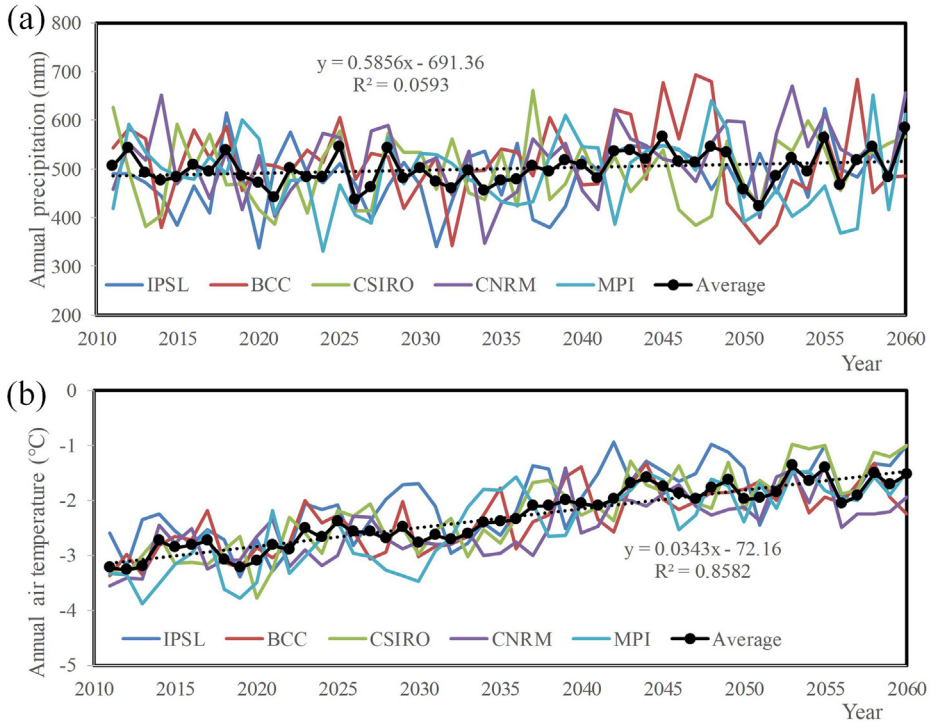

Fig. 3. (a) Annual precipitation and (b) annual mean air temperature in the future 5 decades (2011–2060) based on different GCMs (after correction).

Table 2
Changes in glaciers and frozen soils in the future 5 decades (2011–2060) under the RCP4.5 scenario based on GBEHM outputs.

	IPSL	BCC	CSIRO	CNRM	MPI	Average
Glacier reserve in 2050s (Million m^3)	28	80	34	95	87	65
Permafrost area change percentage	−20%	−21%	−26%	−17%	−31%	−23%
MTSFG (cm/10a)	−6.7	−4.9	−6.0	−3.0	−6.6	−5.4
Active layer depth (cm/10a)	3.4	8.5	7.1	3.5	8.1	6.1

Note: For convenience, the names of the GCMs are simplified as IPSL, BCC, CSIRO, CNRM, MPI and NCEP. The same below.

(476 mm). However, the runoff in the future (124–159 mm based on different GCMs, 138 mm on average) is less than that in the past (165 mm). More precipitation will be lost via evapotranspiration (356–363 mm based on different GCMs, 360 mm on average in the future, and 312 mm in the past). Additionally, the runoff coefficient will be smaller in the future (0.28 on average) than that in the past (0.35).

Table 4 shows the trends of runoff coefficients over the future 50 years in different elevation zones based on different GCMs. The four elevation zones from low to high include the low-altitude vegetation-sparse area (less than 2800 m), highly vegetated area (2800–3600 m), permafrost degradation area (3600–3900 m) and high-altitude permafrost area (> 3900 m). The results show that the runoff coefficient decreases in each elevation zone. The most dramatic decrease occurs in the elevation zone from 3600 to 3900 m, indicating that the degradation process from permafrost to seasonal frozen ground significantly influences the related hydrological processes. Additionally, permafrost degradation increases infiltration and groundwater leakage, leading to a decrease in surface runoff.

4.4. Impacts of precipitation and air temperature changes on annual runoff and evapotranspiration

Table 5 shows the precipitation and air temperature elasticities of runoff/evapotranspiration and the runoff and evapotranspiration changes estimated using the average elasticities in the future 50 years (2011–2060) under the RCP4.5 scenario in comparison with those in the previous 30 years (1981–2010). The results show that when precipitation increases by one unit (1 mm), runoff will increase by 0.72 mm on average (0.53–0.90 mm based on different GCMs), and evapotranspiration will increase by 0.18 mm on average (0.06–0.27 mm based on different GCMs) in the future. These values are similar to the

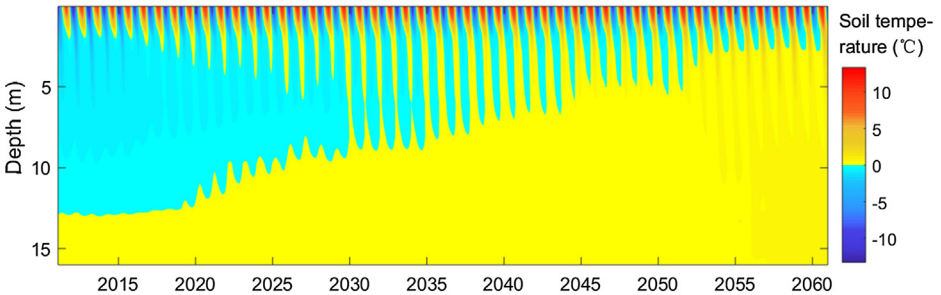

Fig. 4. Changes in spatially averaged monthly ground temperatures in the elevation range between 3600 and 3900 m from 2011 to 2060 (the average simulated value of the 5 GCMs).

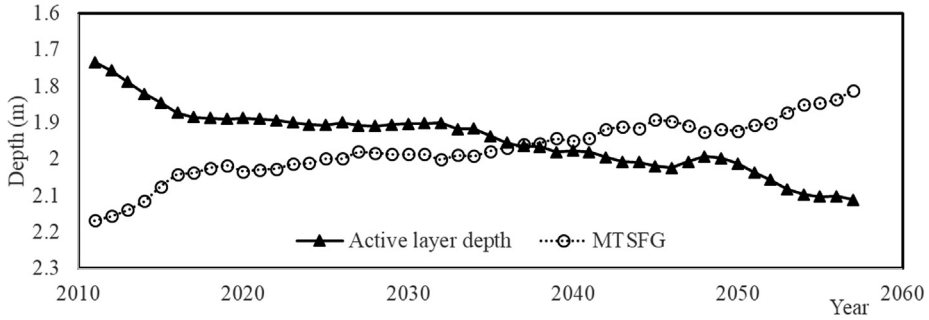

Fig. 5. A 5-year moving average of the simulated (a) active layer depth of permafrost and (b) MTSFG from 2011 to 2060 (the mean value of simulations based on the 5 GCMs).

historical observations (runoff increase by 0.66 mm and evapotranspiration increase by 0.14 mm). When the air temperature rises by 1 °C, runoff will decrease by 24 mm on average (15–40 mm based on different GCMs), and evapotranspiration will increase by 21 mm on average (15–32 mm based on different GCMs). These values that are notably higher absolute values than those in the past based on historical observations (runoff decrease by 6.8 mm and evapotranspiration increase by 11.8 mm). This result indicates that runoff and evapotranspiration may be more sensitive to air temperature increases in the future. In addition to the increase in potential evaporation as the air temperature rises, the increase in air temperature may indirectly affect some hydrological processes. The runoff and evapotranspiration changes in the future based on the average elasticities indicate that decreased runoff and increased evapotranspiration in the future are mainly due to the temperature increase because the future precipitation change is not significant.

Future climate change is associated with considerable uncertainties. Table 1 shows that the climate change trends obtained from different GCMs are considerably different. However, there is a general consensus that warming will continue in the future. Consequently, understanding the response of hydrological processes to the rising air temperature is very important. Based on the estimated air temperature elasticities of runoff/evapotranspiration in the future, we can directly estimate the runoff and evapotranspiration changes under different increased temperature scenarios. Table 6 shows the air temperature trends and their effects on runoff and evapotranspiration changes estimated using the average elasticities (shown in Table 5) under different emission scenarios (RCP 2.6, RCP 4.5 and RCP 8.5) in the future 50 years

Table 3
The average water balance components over the future 50 years (2011–2060) based on different GCMs under the RCP4.5 scenario in comparison to those over the past 30 years (1981–2010).

	IPSL	BCC	CSIRO	CNRM	MPI	Average	1981–2010
Precipitation (mm)	486	508	492	518	488	498	476
Runoff depth (mm)	124	141	135	159	131	138	165
Evapotranspiration (mm)	357	363	356	362	361	360	312
Runoff coefficient	0.26	0.28	0.27	0.31	0.27	0.28	0.35

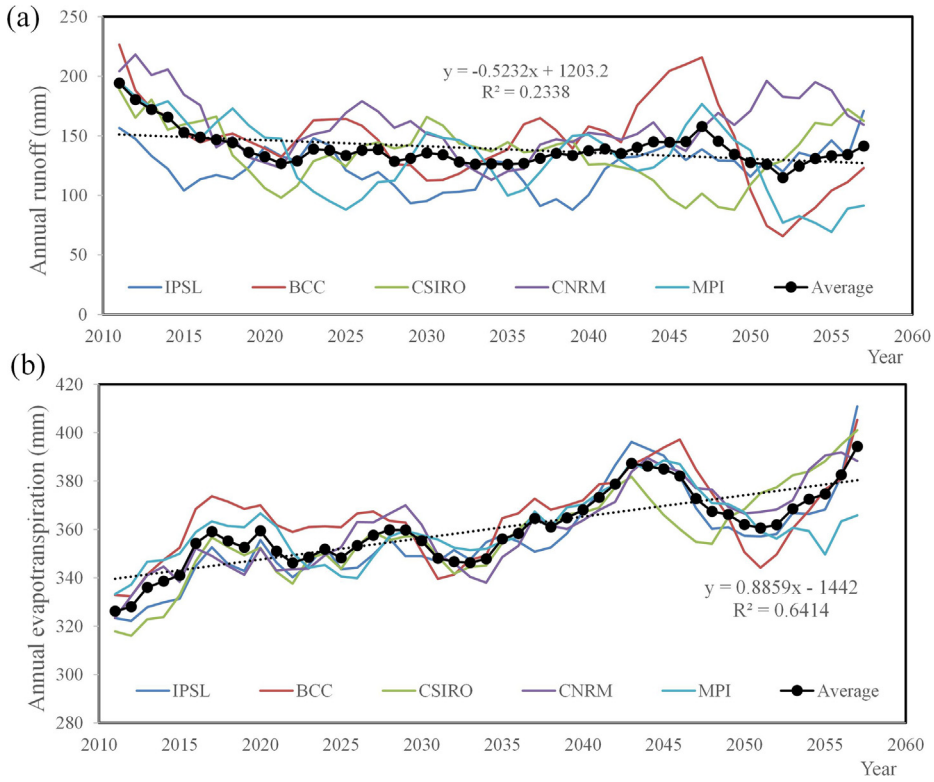

Fig. 6. Five-year moving average of simulated (a) annual runoff and (b) annual evapotranspiration in the future 5 decades (2011–2060) based on different GCMs.

Table 4
The trends of runoff coefficients over the future 50 years (2011–2060) in different elevation zones based on different GCMs under the RCP4.5 scenario (units of "/10a").

Elevation (m)	IPSL	BCC	CSIRO	CNRM	MPI
less than2800	−0.005	−0.002	−0.006	−0.007	−0.007
2800–3600	−0.003	−0.010	−0.018	−0.008	−0.016
3600–3900	**−0.009**	**−0.021**	**−0.023**	**−0.008**	**−0.025**
> 3900	−0.007	−0.020	−0.020	−0.007	−0.023

(2011–2060) in comparison with those in the past (1981–2010). The average rates of air temperature increases in the future are approximately 0.26 °C/10a (RCP 2.6), 0.34 °C/10a (RCP 4.5) and 0.40 °C/10a (RCP8.5) in the HRB (or the northeastern Tibetan Plateau, Su et al., 2016; Zhang et al., 2016a). According to the elasticities, runoff would decrease at a rate of 6 mm/10a under RCP 2.6 scenario, 8 mm/10a under RCP 4.5 scenario, and 10 mm/10a under RCP 8.5 scenario, and evapotranspiration would increase at a rate of 6 mm/10a under RCP 2.6 scenario, 7 mm/10a under RCP 4.5 scenario, and 8 mm/10a under RCP 8.5 scenario.

4.5. Impact of changes in the active layer depth of permafrost on hydrological processes

Table 7 gives the potential evaporation and active layer depth elasticities of runoff and evapotranspiration in the future 50 years (2011–2060). The results show that when potential evaporation increases by one unit (1 mm), runoff will decrease by approximately 0.16 mm on average (0.03–0.28 mm based on different GCMs), and evapotranspiration will increase by approximately 0.3 mm on average (0.14–0.51 mm based on different GCMs). When the active layer depth of permafrost increases by one unit (1 cm), runoff will decrease by approximately 1.3 mm on average (0.6–2.3 mm based on different GCMs), and evapotranspiration will increase by approximately 0.9 mm on average (0.1–1.7 mm based on different GCMs).

Table 8 shows the effects of changes in potential evaporation and the active layer depth on annual runoff and evapotranspiration in the future 50 years (2011–2060), which were estimated based on the average elasticities shown in Table 7. The results show that both the potential evaporation change and the active layer depth change contribute to the runoff decrease and evapotranspiration increase, and the contribution of the active layer depth change is notably higher than the contribution of the potential evaporation change, especially for annual runoff. In addition, the aggregate effects of potential evaporation and active layer depth changes on runoff and evapotranspiration are given in Table 8 for comparison with the air temperature influences shown in Table 5. The results indicate that the two values are similar (although the results from each individual GCM may have some bias because the average elasticities cannot perfectly represent the elasticities of each GCM). Thus, the assumption that the impacts of air temperature change can be divided into the impact of the potential evaporation change and the impact of the active layer depth change is reasonable. Consequently, we can conclude that the main influence of the air temperature change on runoff is associated with the change in the active depth of the frozen soil rather than the change in potential evaporation. The rising temperature thickens the active layer depth of the frozen ground, leading to an increase in the soil storage capacity and changing the mechanism of runoff production.

Table 6
Air temperature trends and their effects on runoff and evapotranspiration changes estimated using the average elasticities under different emission scenarios (RCP 2.6, RCP 4.5 and RCP 8.5) in the future 50 years (2011–2060) in comparison with those in the past (1981–2010).

	Future (2011–2060)			Past 3-decades 1981–2010
	RCP 2.6	RCP 4.5	RCP 8.5	
ΔT (°C/10a)	0.26	0.34	0.40	0.32
$\Delta R_T = \overline{\varepsilon'_{T,R}}\cdot\Delta T$ (mm/10a)	−6	−8	−10	−2.1
$\Delta ET_T = \overline{\varepsilon'_{T,ET}}\cdot\Delta T$ (mm/10a)	6	7	8	3.7

Table 7
Potential evapotranspiration and active layer depth elasticities of runoff/evapotranspiration in the future 50 years (2011–2060).

	IPSL	BCC	CSIRO	CNRM	MPI	Average
$\varepsilon'_{PET,R}$ (mm/mm)	−0.03*	−0.18	−0.16	−0.17	−0.28	−0.16
$\varepsilon'_{D,R}$(mm/cm)	−1.8	−0.6	−1.2	−2.3	−0.6	−1.3
$\varepsilon'_{PET,ET}$ (mm/mm)	0.15	0.34	0.14	0.35	0.51	0.30
$\varepsilon'_{D,ET}$(mm/cm)	1.7	0.3	1.1	1.4	0.1*	0.9

Note: "*" means that the correlation of the two items is not significant ($\alpha = 0.1$).

Table 8
Runoff and evapotranspiration changes caused by potential evapotranspiration (PET) and active layer depth (D) changes in the future 50 years (2011–2060) under the RCP4.5 scenario estimated using the average elasticities.

	IPSL	BCC	CSIRO	CNRM	MPI	Average
$\Delta R_{PET} = \overline{\varepsilon'_{PET,R}}\cdot\Delta PET$ (mm/10a)	−2.0	−1.6	−2.6	−1.7	−2.2	−2.0
$\Delta R_D = \overline{\varepsilon'_{D,R}}\cdot\Delta D$ (mm/10a)	−4.5	−11.2	−9.4	−4.6	−10.7	−8.1
$\Delta R_{PET} + \Delta R_D$ (mm/10a)	−6.5	−12.9	−12.0	−6.3	−12.9	−10.1
$\Delta ET_{PET} = \overline{\varepsilon'_{PET,ET}}\cdot\Delta PET$ (mm/10a)	3.8	3.1	4.9	3.1	4.1	3.8
$\Delta ET_D = \overline{\varepsilon'_{D,ET}}\cdot\Delta D$ (mm/10a)	3.1	7.7	6.4	3.2	7.3	5.5
$\Delta ET_{PET} + \Delta ET_D$ (mm/10a)	6.8	10.7	11.3	6.3	11.4	9.3

Table 5
Precipitation and air temperature elasticities of runoff/evapotranspiration and runoff and evapotranspiration changes estimated using the average elasticities in the future (2011–2060) under the RCP4.5 scenario in comparison with those in the past (1981–2010).

	Future (2011–2060)						Past 3-decades
	IPSL	BCC	CSIRO	CNRM	MPI	Average	1981–2010
$\varepsilon'_{P,R}$ (mm/mm)	0.53	0.68	0.83	0.90	0.66	0.72	0.66
$\varepsilon'_{T,R}$ (mm/°C)	−14.8	−22.5	−24.8	−39.9	−18.0	−24.0	−6.8
$\varepsilon'_{P,ET}$(mm/mm)	0.27	0.23	0.10	0.06	0.22	0.18	0.14
$\varepsilon'_{T,ET}$(mm/°C)	17.1	18.3	23.9	32.4	15.1	21.4	11.8
$\Delta R_P = \overline{\varepsilon'_{P,R}}\cdot\Delta P$ (mm/10a)	10.8	−0.8	5.3	8.9	−4.2	4.0	7.4
$\Delta R_T = \overline{\varepsilon'_{T,R}}\cdot\Delta T$(mm/10a)	−8.2	−6.7	−10.1	−6.5	−9.6	−8.2	−2.1
$\Delta ET_P = \overline{\varepsilon'_{P,ET}}\cdot\Delta P$(mm/10a)	2.6	−0.2	1.3	2.2	−1.0	1.0	1.6
$\Delta ET_T = \overline{\varepsilon'_{T,ET}}\cdot\Delta T$ (mm/10a)	7.3	6.0	9.0	5.8	8.5	7.3	3.7

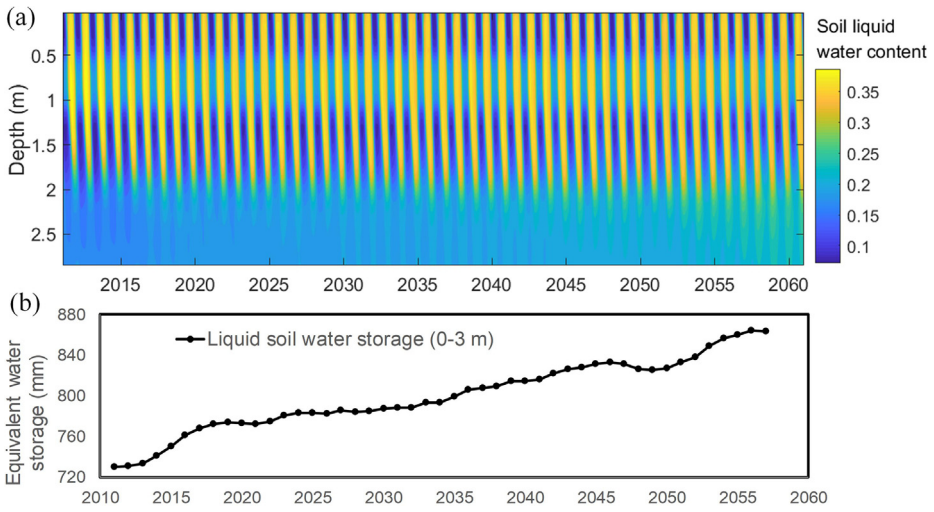

Fig. 7. Changes in the simulated (a) basin-averaged monthly soil liquid water content, and (b) basin-averaged annual soil liquid water storage (equivalent water depth) in the 0–3 m soil layer below the ground surface (the average simulated value of the 5 GCMs).

5. Discussion

5.1. Impact of frozen ground degradation on runoff change

In the upper HRB, precipitation is mainly concentrated in the summer, and the soil in summer is largely saturated. The main runoff production mechanism in the upper HRB is excess saturation. In addition, precipitation increases significantly with elevation in the upper HRB (Wang et al., 2017); therefore, runoff is mainly generated at high latitudes, and the permafrost region and transition region from permafrost to seasonally frozen ground contribute the most to runoff in the upper HRB (Gao et al., 2016). According to the results in Section 4, the effects of the degradation of frozen soil in these two regions on the runoff change are different. In permafrost areas, the thickening of the active layer increases the soil storage capacity. Fig. 7 shows the change in simulated monthly basin-averaged soil liquid water from 2011 to 2060 and the change in the annual soil liquid water equivalent. The results show that the soil liquid water content significantly increases in the next 50 years and that the lower boundary of soil liquid water becomes deeper due to the impact of active layer changes on the soil water capacity. The annual soil liquid water equivalent displays a significant increasing trend, and the associated changes are highly correlated with the changes in the active layer depth of permafrost (Fig. 5), with a correlation coefficient (R^2) equal to 0.98. This finding also indicates that the change in the active layer depth has a significant effect on soil moisture. Due to the main runoff production mode in the upper HRB is saturation-excess runoff, the increase in the soil storage capacity significantly impacts runoff (decrease) and evapotranspiration (increase). In the transition areas, the change from permafrost to seasonal frozen ground increases groundwater infiltration, leading to an increase in liquid soil moisture in the deep layers and a decrease in surface runoff. Notably, frozen ground degradation causes an increase in the water storage capacity, thereby changing the runoff mechanism. Cao et al. (2012) analyzed the change in the soil storage capacity in the HRB from 2003 to 2008 based on GRACE data and observed an increasing trend, which is consistent with our conclusion.

In previous studies, climate change was often considered based on changes in precipitation and drought indexes (namely, potential evaporation divided by precipitation); therefore, the impacts of climate change on runoff change were divided between the impact of precipitation change and the impact of potential evaporation change (e.g., the Budyko-based approach; Budyko, 1974; Yang and Yang, 2011; Xu et al., 2014; Zhang et al., 2016b). However, in cold areas, in addition to the effects of precipitation change and potential evaporation change, the influence of frozen ground changes on runoff is also important (even more important than the effects of precipitation and potential evaporation changes, according to the results in Section 4.5). Consequently, it is necessary to consider the effect of frozen ground change when analyzing the influences of climate change on runoff in future studies.

5.2. Differences in frozen ground changes in the past and future

Over the past 30 years (1981–2010), the increasing air temperature trend was approximately 0.33 °C/10a. Based on the GBEHM simulation result (Gao et al., 2018), the maximum frozen depth of seasonally frozen ground decreased by approximately 4.1 cm/10a, and the active layer depth increased by approximately 2.2 cm/10a over the past 30 years. These results were validated based on the gauge observations from national meteorological stations (Wang et al., 2013; Wu and Zhang, 2010; Peng et al., 2017).

The rate of increase in air temperature over the future 50 years (approximately 0.34 °C/10a estimated in this study) in the upper HRB is close to the historical value. However, both the decrease in the maximum frozen depth of seasonally frozen ground and thickening of the active layer of permafrost are projected to accelerate in the future (−5.4 cm/10a and 6.1 cm/10a, respectively) compared with the rates in the past. This difference partially explains why the absolute values of the air temperature elasticities of annual runoff/evapotranspiration in the future are much higher than those in the past, as shown in Table 5. Thus, the hydrological changes in the HRB are highly sensitive to the increase in air temperature due to the degradation of frozen ground.

5.3. Comparison with previous similar studies

This study is a follow up to the series of studies of our research group. In our previous studies, we used an empirical model and a physical model to estimate the effects of climate change on frozen ground and the impacts of frozen ground degradation on hydrological processes, respectively. Based on the empirical model (the Budyko framework), we conducted an attribution analysis of the runoff changes in a frozen ground region in the context of climate change (Wang et al., 2018). The research distinguished the effects of changes in precipitation, potential evaporation, frozen ground, and land use on runoff changes, and the conclusion that frozen ground change had a significant effect on the change in runoff was obtained. However, the study by Wang et al. (2018) did not quantitatively provide the air temperature elasticity of runoff and the frozen ground elasticity of

runoff; therefore, the effects of air temperature change on runoff in the future could not be assessed. Based on the physical model (GBHEM), Gao et al. (2018) simulated the changes in frozen ground and the changes in hydrological processes based on historical climate trends. The study explained the physical mechanisms of the impact of warming on frozen ground and the impacts of frozen ground degradation on hydrological processes. The current study is an extension of Gao's research. Based on GBEHM, we simulated the changes in frozen ground and runoff under typical climate scenarios in the future. Based on the simulation results, we estimated the air temperature elasticity of runoff and the frozen ground elasticity of runoff. Then, according to the elasticities, we quantitatively estimated the changes in frozen ground and runoff under different increased temperature scenarios in the future.

This study shows that the degradation of frozen ground in the upper HRB increases infiltration and soil water storage, which subsequently increases evapotranspiration and reduces runoff. The degradation of frozen ground leads to an increase in soil water storage, which is consistent with the results of several previous studies, including studies in Arctic Alaska (McNamara et al. 1998), North America (Lyon and Destouni, 2010), Austria (Rogger et al., 2017) and the Tibetan Plateau region (Cuo et al. 2015; Gao et al., 2018). However, the conclusion that permafrost deterioration will lead to a reduction in runoff varies in different regions. For example, previous studies in the source regions of the Yellow River (Jin et al., 2009) and Yangtze River (Qiu, 2012) showed that the degradation of permafrost can lead to a decrease in runoff, which was the cause of the thickening of the active layer of permafrost (Qiu, 2012). These conclusions are consistent with the findings of this study. Studies by Lyon et al. (2009) in North America and Rogger et al. (2017) in Austria suggested that the degradation of permafrost increases the melting of soil ice, which leads to an increase in runoff. This difference may be related to climatic differences. The climate of the upper HRB is relatively dry, and previous studies showed that there is little soil ice in the frozen soils of the region (Gao et al., 2018).

In recent years, Zhang et al. (2016a) and Chen et al. (2018) also analyzed the future cryospheric and hydrological changes in the upper HRB based on different hydrological models. Chen et al. (2018) showed that the glaciers in the upper HRB could disappear in the future, which is consistent with the findings of the present study. Both studies stated that future runoff would increase due to increased precipitation. The two studies also noted that future precipitation is associated with considerable uncertainty. Compared with these previous studies, the present study quantified the impact of the accelerated degradation of the frozen soils caused by the air temperature increase on future runoff and evapotranspiration. This research shows that the effects of permafrost degradation on runoff are greater than the impacts of glacier melt and snow melt in the upper HRB. All GCMs projected increases in the future air temperature. Thus, regardless of how precipitation changes in the future, the degradation of permafrost caused by increased air temperatures is projected to significantly reduce runoff and potentially result in water resource shortages in the lower reaches of the study area.

5.4. Uncertainty and limitations

The sources of uncertainty in this study include the climate models, the downscaling and bias correction methods, and the structure and parameters of the ecohydrological model (Wilby and Harris, 2006). Because future climate simulations are uncertain, the low spatial accuracy of the GCMs leads to difficulty in reflecting the spatial variability of the climate in mountainous areas. Despite the application of downscaling and bias correction methods, the high-resolution spatial patterns of the climate factors such as precipitation and air temperature are difficult to perfectly represent. Uncertainties with respect to the choice of model parameterization in the ecohydrological simulation are another complicated source of error. Since the terrain conditions in mountainous areas are complex, the inhomogeneity among factors such as surface albedo, soil type, soil depth, land use type and vegetation cover may not be fully captured at the regional scale. Moreover, soil water and heat parameters can affect ecohydrological simulations. The above uncertainties lead to variations in the conclusions obtained based on different climate models. To reduce the impacts of these uncertainties, this study adopted an ensemble estimation based on multiple GCMs. Future improvement of the GCMs and the consideration of additional data could greatly reduce these uncertainties.

6. Conclusion

Based on 5 typical future climate scenarios (under emission scenario RCP4.5), this study employed a distributed ecohydrological model (GBEHM) to analyze the potential future climate change (from 2011 to 2060) and the associated impacts on the cryospheric and hydrological processes in the upper HRB. According to the simulation results, the following conclusions can be drawn.

1. The air temperature is projected to rise by approximately 0.34 °C/10a, and precipitation is projected to slightly increase by approximately 6 mm/10a in the future under RCP 4.5 scenario. By 2060, glaciers would comprise a volume of less than 100 million m^3, the permafrost area would shrink by approximately 23%, the maximum frozen depth of seasonally frozen ground would decrease by approximately 5.4 cm/10a, and the active layer depth over the permafrost would increase by approximately 6.1 cm/10a.
2. Due to climate change, runoff is projected to decrease by approximately 5 mm/10a, and evapotranspiration is projected to increase by approximately 9 mm/10a. The average increases in annual precipitation, runoff and ET over the future 50 years are estimated to be 498 mm, 138 mm and 360 mm, respectively. This average runoff is only 80% of that in the 2000s. The average runoff coefficient over the future 50 years is 0.28, and the decrease in the runoff coefficient is greatest in the elevation zone of 3600–3900 m, where permafrost degrades and becomes seasonal frozen ground.
3. Over the future 50 years, the changes in hydrological processes are mainly due to the increase in the air temperature, with average changes of −24 mm/°C for runoff and 21 mm/°C for evapotranspiration. The effects of air temperature changes on runoff and evapotranspiration are largely dominated by changes in frozen ground. The first associated mechanism is the thickening of the active layer, which increases the soil storage capacity and leads to a decrease in runoff and increase in evapotranspiration. When the active layer depth increases by 1 cm, runoff will decrease by approximately 1.3 mm, and evapotranspiration will increase by approximately 0.9 mm. The other mechanism involves changes from permafrost to seasonal frozen ground, which increase groundwater infiltration and the volume of liquid soil moisture in the deep layers and decrease surface runoff.
4. The frozen ground in the upper HRB is more sensitive to temperature increases in the future than those in the past. This trend leads to a faster reduction in runoff in the future based on the same rate of temperature increase.
5. The elasticities obtained in this study can be utilized to estimate the runoff changes in different climate scenarios. Based on these elasticities, future runoff would decrease at rates of approximately 6 mm/10a, 8 mm/10a, and 10 mm/10a under the emission scenarios of RCP 2.6, RCP 4.5, and RCP 8.5, respectively. Additionally, and evapotranspiration would increase at rates of approximately 6 mm/10a, 7 mm/10a, and 8 mm/10a under these three emission scenarios.

In this study, we did not consider vegetation changes in the future. However, the interactions among vegetation growth, cryospheric

processes and hydrological processes could be important. Therefore, the effects of vegetation dynamics should be considered in future studies.

Acknowledgements

This research was supported by grants from the National Natural Science Foundation of China (Project Nos. 91225302 and 91425303).

References

Bales, R.C., Molotch, N.P., Painter, T.H., Dettinger, M.D., Rice, R., Dozier, J., 2006. Mountain hydrology of the western United States. Water Resour. Res. 42 (8).
Barry, R., Gan, T.Y., 2011. Global Cryosphere-Past, Present and Future. New York, Cambridge University Press.
Boé, J., Terray, L., Habets, F., Martin, E., 2007. Statistical and dynamical downscaling of the Seine basin climate for hydro-meteorological studies. Int. J. Climatol. 27 (12), 1643–1655.
Bosson, E., Sabel, U., Gustafsson, L., Sassner, M., Destouni, G., 2012. Influences of shifts in climate, landscape, and permafrost on terrestrial hydrology. J. Geophys. Res. Atmos. 117(D5). https://doi.org/10.1029/2011JD016429.
Budyko, M., 1974. Climate and life. Academic Press, New York, NY.
Cao, Y., Nan, Z., Hu, X., 2012. Changes of Groundwater Storage in the Heihe River Basin Derived from GRACE Gravity Satellite Data. J. Glaciol. Geocryol. 3, 680–689.
Chen, R., Wang, G., Yang, Y., Liu, J., Han, C., Song, Y., Liu, Z., Kang, E., 2018. Effects of Cryospheric Change on Alpine Hydrology: Combining a Model with Observations in the Upper Reaches of the Hei River, China. J. Geophys. Res. Atmos. https://doi.org/10.1002/2017JD027876.
Cheng, G., Wu, T., 2007. Responses of permafrost to climate change and their environmental significance, Qinghai-Tibet Plateau. J. Geophys. Res. 112 (F2). https://doi.org/10.1029/2006JF000631.
Cheng, G., Jin, H., 2013. Permafrost and groundwater on the Qinghai-Tibet Plateau and in northeast China. Hydrogeol. J. 21 (1), 5–23.
Chiew, F., Peel, M.C., Mcmahon, T.A., Siriwardena, L.W., Demuth, S., 2006. Precipitation elasticity of streamflow in catchments across the world. IAHS publication 308, 256–262.
Cuo, L., Zhang, Y., Zhu, F., Liang, L., 2014. Characteristics and changes of streamflow on the Tibetan Plateau: a review. J. Hydrol. Reg. Stud. 2, 49–68.
Cuo, L., Zhang, Y., Bohn, T.J., Zhao, L., Li, J., Liu, Q., Zhou, B., 2015. Frozen soil degradation and its effects on surface hydrology in the northern Tibetan Plateau. J. Geophys. Res. Atmos. 120 (16), 8276–8298.
Fan, W., 2014. Heihe 1km LAI production. Heihe Plan Science Data Center at Lanzhou. https://doi.org/10.3972/heihe.090.2014.db.
Fowler, H.J., Blenkinsop, S., Tebaldi, C., 2007. Linking climate change modelling to impacts studies: recent advances in downscaling techniques for hydrological modelling. Int. J. Climatol. 27 (12), 1547–1578. https://doi.org/10.1002/joc.1556.
Fu, B., 1981. On the Calculation of the Evaporation from Land Surface. Scientia Atmospherica Sinica 5, 23–31.
Fu, G., Liu, Z., Charles, S.P., Xu, Z., Yao, Z., 2013. A score-based method for assessing the performance of GCMs: A case study of southeastern Australia. J. Geophys. Res.: Atmos. 118 (10), 4154–4167. https://doi.org/10.1002/jgrd.50269.
Gao, B., 2012. Land-Atmosphere Coupling Simulation and Analysis of Streamflow Changes in the Yangtze River Basin. Tsinghua University.
Gao, B., Qin, Y., Wang, Y., Yang, D., Zheng, Y., 2016. Modeling Ecohydrological Processes and Spatial Patterns in the Upper Heihe Basin in China. Forests 7 (1), 10. https://doi.org/10.3390/f7010010.
Gao, B., Yang, D., Qin, Y., Wang, Y., Li, H., Zhang, Y., Zhang, T., 2018. Change in frozen soils and its effect on regional hydrology, upper Heihe basin, northeastern Qinghai-Tibetan Plateau. The Cryosphere 12 (2), 657–673. https://doi.org/10.5194/tc-12-657-2018.
Guo, W., Xu, J., Liu, S., Shangguan, D., Wu, L., Yao, X., Zhao, J., Liu, Q., Jiang, Z., Li, P., Wei, J., Bao, W., Yu, P., Ding, L., Li, G., Ge, C., Wang, Y., 2014. In: Cold and Arid Regions Science Data Center at Lanzhou, https://doi.org/10.3972/glacier.001.2013.db.
Hu, Q., Jiang, D., Fan, G., 2014. Evaluation of CMIP5 Models over the Qinghai-Tibetan Plateau. Chin. J. Atmos. Sci. 38 (05), 924–938 (in Chinese).
Immerzeel, W.W., van Beek, L.P.H., Bierkens, M.F.P., 2010. Climate Change Will Affect the Asian Water Towers. Science 328 (5984), 1382–1385.
Immerzeel, W.W., van Beek, L.P.H., Konz, M., Shrestha, A.B., Bierkens, M.F.P., 2012. Hydrological response to climate change in a glacierized catchment in the Himalayas. Clim. Change 110 (3–4), 721–736.
[dataset] Jarvis, A., Reuter, H. I., Nelson, A., and Guevara, E., 2008. Hole-filled SRTM for the globe Version 4. [Available online from the CGIAR-CSI SRTM 90m Databaseat http://srtm.csi.cgiar.org.].
Jin, H., He, R., Cheng, G., Wu, Q., Wang, S., Lü, L., Chang, X., 2009. Changes in frozen ground in the Source Area of the Yellow River on the Qinghai–Tibet Plateau, China, and their eco-environmental impacts. Environ. Res. Lett. 4, 045206. https://doi.org/10.1088/1748-9326/4/4/045206.
Kang, S., Xu, Y., You, Q., Flügel, W., Pepin, N., Yao, T., 2010. Review of climate and cryospheric change in the Tibetan Plateau. Environ. Res. Lett. 5, 015101.
Konapala, G., Mishra, A.K., 2016. Three-parameter-based streamflow elasticity model: application to MOPEX basins in the USA at annual and seasonal scales. Hydrol. Earth Syst. Sci. 20 (6), 2545–2556.
Lawrence, D.M., Koven, C.D., Swenson, S.C., Riley, W.J., Slater, A.G., 2015. Permafrost thaw and resulting soil moisture changes regulate projected high-latitude CO2 and CH4 emissions. Environ. Res. Lett. 10 (9). https://doi.org/10.1088/1748-9326/10/9/094011.
Lyon, S.W., Destouni, G., 2010. Changes in Catchment-Scale Recession Flow Properties in Response to Permafrost Thawing in the Yukon River Basin. Int. J. Climatol. 30 (14), 2138–2145. https://doi.org/10.1002/joc.1993.
Lyon, S.W., Destouni, G., Giesler, R., Humborg, C., Morth, M., Seibert, J., Karlsson, J., Troch, P.A., 2009. Estimation of permafrost thawing rates in a sub-arctic catchment using recession flow analysis. Hydrol. Earth Syst. Sc. 13, 595–604. https://doi.org/10.5194/hess-13-595-2009.
Ma, H., Yang, D., Tan, S.K., Gao, B., Hu, Q., 2010. Impact of climate variability and human activity on streamflow decrease in the Miyun Reservoir catchment. J. Hydrol. 389 (3–4), 317–324.
McNamara, J.P., Kane, D.L., Hinzman, L.D., 1998. An analysis of streamflow hydrology in the Kuparuk River Basin, Arctic Alaska: a nested watershed approach. J. Hydrol. 206 (1), 39–57. https://doi.org/10.1016/S0022-1694(98)00083-3.
New, M., Hulme, M., Jones, P., 2000. Representing Twentieth-Century Space–Time Climate Variability. Part II: Development of 1901–96 Monthly Grids of Terrestrial Surface Climate, 13(13) 2217–2238. doi:10.1175/1520-0442(2000)013 < 2217:RTCSTC > 2.0.CO;2.
Ning, B., He, Y., He, X., Li, Z., 2008. Advances on Water Resources Research in Heihe River Basin. J. Desert Res. 28 (6), 1180–1185 (in Chinese).
Peng, X., Zhang, T., Frauenfeld, O.W., Wang, K., Cao, B., Zhong, X., Su, H., Mu, C., 2017. Response of seasonal soil freeze depth to climate change across China. The Cryosphere 11 (3), 1059–1073. https://doi.org/10.5194/tc-11-1059-2017.
Qin, Y., Lei, H., Yang, D., Gao, B., Wang, Y., Cong, Z., Fan, W., 2016. Long-term change in the depth of seasonally frozen ground and its ecohydrological impacts in the Qilian Mountains, northeastern Tibetan Plateau. J. Hydrol. 542, 204–221.
Qiu, J., 2012. Thawing permafrost reduces river runoff. Nature News. https://doi.org/10.1038/nature.2012.9749.
Rogger, M., Chirico, G.B., Hausmann, H., Krainer, K., Brückl, E., Stadler, P., Blöschl, G., 2017. Impact of mountain permafrost on flow path and runoff response in a high alpine catchment. Water Resour. Res. 53 (2), 1288–1308. https://doi.org/10.1002/2016WR019341.
Sankarasubramanian, A., Vogel, R.M., Limburner, J.F., 2001. Climate elasticity of streamflow in the United States. Water Resour. Res. 37 (6), 1771–1781. https://doi.org/10.1029/2000WR900330.
Schaake, J.C., 1990. In: Waggoner, P.E. (Ed.), From Climate to Flow in Climate Change and US Water Resources. John Wiley, New York, pp. 177–206 (Chapter 8).
Song, X., Brus, D.J., Liu, F., Li, D., Zhao, Y., Yang, J., Zhang, G., 2016. Mapping soil organic carbon content by geographically weighted regression: a case study in the Heihe River Basin, China. Geoderma 261, 11–22. https://doi.org/10.1016/j.geoderma.2015.06.024.
Su, F., Zhang, L., Ou, T., Chen, D., Yao, T., Tong, K., Qi, Y., 2016. Hydrological response to future climate changes for the major upstream river basins in the Tibetan Plateau. Global Planet. Change 136, 82–95. https://doi.org/10.1016/j.gloplacha.2015.10.012.
Wang, L., Koike, T., Yang, K., Jin, R., Li, H., 2010. Frozen soil parameterization in a distributed biosphere hydrological model. Hydrol. Earth Syst. Sci. 14 (3), 557–571. https://doi.org/10.5194/hess-14-557-2010.
Wang, Q., Zhang, T., Wu, J., Peng, X., Zhong, X., Mu, C., Wang, K., Wu, Q., Cheng, G., 2013. Investigation of permafrost distribution over the upper reaches of the heihe River in the Qilian Mountains. J. Glaciol. Geocryol. 35 (1), 19–29 (in Chinese).
Wang, T., Yang, H., Yang, D., Qin, Y., Wang, Y., 2018. Quantifying the streamflow response to frozen ground degradation in the source region of the Yellow River within the Budyko framework. J. Hydrol. 558, 301–313. https://doi.org/10.1016/j.jhydrol.2018.01.050.
Wang, Y., Yang, D., Lei, H., Yang, H., 2015. Impact of cryosphere hydrological processes on the river runoff in the upper reaches of Heihe River. J. Hydraul. Eng. 46 (9), 1064–1071 (in Chineses).
Wang, Y., Yang, H., Yang, D., Qin, Y., Gao, B., Cong, Z., 2017. Spatial Interpolation of Daily Precipitation in a High Mountainous Watershed Based on Gauge Observations and a Regional Climate Model Simulation. J. Hydrometeorol. 18 (3), 845–862. https://doi.org/10.1175/JHM-D-16-0089.1.
Wilby, R.L., Harris, I., 2006. A framework for assessing uncertainties in climate change impacts: low-flow scenarios for the River Thames, UK. Water Resour. Res. 42(2). doi:10.1029/2005WR004065.
Willmott, C.J., Rowe, C.M., Philpot, W.D., 1985. Small-Scale Climate Maps: A Sensitivity Analysis of Some Common Assumptions Associated with Grid-Point Interpolation and Contouring 12 (1), 5–16. https://doi.org/10.1559/152304085783914686.
Woo, M.K., 2012. Permafrost Hydrology. Springer-Verlag, Berlin Heidelberg.
Wood, A.W., 2002. Long-range experimental hydrologic forecasting for the eastern United States. J. Geophys. Res. 107 (D20).
Wood, A.W., Leung, L.R., Sridhar, V., Lettenmaier, D.P., 2004. Hydrologic Implications of Dynamical and Statistical Approaches to Downscaling Climate Model Outputs. Clim. Change 62, 189–216. https://doi.org/10.1023/B:CLIM.0000.
Wu, Q. and Zhang, T., 2010. Changes in active layer thickness over the Qinghai-Tibetan Plateau from 1995 to 2007. J. Geophys. Res. 115(D9). doi: 10.1029/2009JD012974.
Xu, X., Yang, D., Yang, H., Lei, H., 2014. Attribution analysis based on the Budyko hypothesis for detecting the dominant cause of runoff decline in Haihe basin. J. Hydrol. 510, 530–540.
Yang, D., Herath, S., Musiake, K., 2002. A hillslope-based hydrological model using catchment area and width functions. Hydrol. Sci. J. 47 (1), 49–65. https://doi.org/10.1080/02626660209492907.
Yang, D., Li, C., Ni, G., Hu, H., 2004. Application of a distributed hydrological model to the Yellow River basin. Acta Geographica Sinica-Chinese Edition 59 (1), 143–154 (in

Chinese).
Yang, D., Gao, B., Jiao, Y., Lei, H., Zhang, Y., Yang, H., Cong, Z., 2015. A distributed scheme developed for eco-hydrological modeling in the upper Heihe River. Sci. China Earth Sci. 58 (1), 36–45.
Yang, H., Yang, D., 2011. Derivation of climate elasticity of runoff to assess the effects of climate change on annual runoff. Water Resour. Res. 47 (7), 197–203.
Yang, K., Ye, B., Zhou, D., Wu, B., Foken, T., Qin, J., Zhou, Z., 2011. Response of hydrological cycle to recent climate changes in the Tibetan Plateau. Clim. Change 109 (3–4), 517–534.
Yao, T., Pu, J., Lu, A., Wang, Y., Yu, W., 2007. Recent Glacial Retreat and Its Impact on Hydrological Processes on the Tibetan Plateau, China, and Surrounding Regions. Arct. Antarct. Alp. Res. 39 (4), 642–650.
Zhang, A., Liu, W., Yin, Z., Fu, G., Zheng, C., 2016a. How Will Climate Change Affect the Water Availability in the Heihe River Basin, Northwest China? J. Hydrometeorol. 17 (5), 1517–1542.
Zhang, S., Yang, D., Jayawardena, A.W., Xu, X., Yang, H., 2016b. Hydrological change driven by human activities and climate variation and its spatial variability in Huaihe Basin. China 61 (8), 1370–1382.
Zhou, J., Zheng, Y., 2014. Vegetation Map of the upper Heihe basin, Version 2.0, Heihe Plan Science Data Center at Lanzhou, China. doi:10.3972/heihe.426.2014.db.